Title

Pumping iron: A multi-omics analysis of two extremophilic algae reveals iron economy management

Journal

Proceedings of the National Academy of Sciences of the United States of America, 120(30)

ISSN

0027-8424

Authors

Davidi, Lital
Gallaher, Sean D
Ben-David, Eyal
et al.

Publication Date

2023-07-25

DOI

10.1073/pnas.2305495120

PNAS RESEARCH ARTICLE | PLANT BIOLOGY OPEN ACCESS

Pumping iron: A multi-omics analysis of two extremophilic algae reveals iron economy management

Lital Davidi[a,1], Sean D. Gallaher[a,b,1,2], Eyal Ben-David[c,3], Samuel O. Purvine[d], Thomas L. Fillmore[d], Carrie D. Nicora[e], Rory J. Craig[b], Stefan Schmollinger[a,4], Sanja Roje[f], Crysten E. Blaby-Haas[g,h], Robert P. Auber[i], Jennifer H. Wisecaver[i], and Sabeeha S. Merchant[a,b,j,k,2]

Contributed by Sabeeha S. Merchant; received April 5, 2023; accepted June 12, 2023; reviewed by Ursula W. Goodenough and Caroline C. Philpott

Marine algae are responsible for half of the world's primary productivity, but this critical carbon sink is often constrained by insufficient iron. One species of marine algae, *Dunaliella tertiolecta*, is remarkable for its ability to maintain photosynthesis and thrive in low-iron environments. A related species, *Dunaliella salina* Bardawil, shares this attribute but is an extremophile found in hypersaline environments. To elucidate how algae manage their iron requirements, we produced high-quality genome assemblies and transcriptomes for both species to serve as a foundation for a comparative multiomics analysis. We identified a host of iron-uptake proteins in both species, including a massive expansion of transferrins and a unique family of siderophore-iron-uptake proteins. Complementing these multiple iron-uptake routes, ferredoxin functions as a large iron reservoir that can be released by induction of flavodoxin. Proteomic analysis revealed reduced investment in the photosynthetic apparatus coupled with remodeling of antenna proteins by dramatic iron-deficiency induction of TIDI1, which is closely related but identifiably distinct from the chlorophyll binding protein, LHCA3. These combinatorial iron scavenging and sparing strategies make *Dunaliella* unique among photosynthetic organisms.

iron homeostasis | phytoplankton | *Chlamydomonas reinhardtii* | iron starvation–induced protein (ISIP) | flavin biosynthesis

Significance

Algae play a huge role in CO_2 uptake via photosynthesis and represent an important target for climate crisis mitigation efforts. Most photosynthesis proteins require iron as a cofactor so that insufficient iron often limits algal CO_2 sequestration. With this in mind, we examined a genus of algae in the green plant lineage called *Dunaliella* that is exceptionally well adapted to low-iron environments. We produced complete genomes, transcriptomes, and proteomes for two species of *Dunaliella* that hail from radically different environments: one from coastal ocean waters and the other from salt flats. We identified dozens of genes and multiple, complementary strategies for iron uptake and management, such as the replacement of ferredoxin by flavodoxin, which reduces the Fe quota by 6%.

The atmospheric release of CO_2 due to human activity represents a grave threat to world ecosystems and human well-being. An important counterbalance to rising greenhouse gas concentrations is primary productivity, wherein CO_2 is taken up by photosynthetic organisms and converted to organic compounds. Approximately one half of primary productivity on Earth is due to the photosynthetic activity of marine algae (1). Unfortunately, this critical carbon sink is constrained by insufficient Fe in approximately one third of the Earth's oceans (2). As evidenced by mesoscale Fe-addition experiments, seeding the water in these high-nutrient–low-chlorophyll regions with Fe is sufficient to induce blooms of phytoplankton (3). Thus, a greater understanding of the role of Fe uptake and homeostasis in algae represents an important research aim for mitigation of the climate crisis.

Not all algae are equally adept at acquiring Fe from their environment. While Fe is the fourth most abundant element in the Earth's crust, it has poor bioavailability (4, 5). In our oxygenated world, Fe reacts with oxygen to form insoluble oxyhydroxides that become inaccessible to many aquatic organisms or energetically costly to access. One genus of green algae that is exceptional at Fe uptake is *Dunaliella*. This genus comprises motile, unicellular green algae of the chlorophyte lineage, which diverged ~500 Mya (6) from the lineage that includes the reference chlorophycean alga, *Chlamydomonas reinhardtii. Dunaliella* species are extremely halotolerant as well as tolerant of extremes of high light, temperature, and a wide range of pH (7). *Dunaliella* species are cosmopolitan in their distribution, including coastal sea waters, salty lakes, and even salt flats (Fig. 1*A*). In lieu of having a rigid cell wall, cells of *Dunaliella* are surrounded by a spongy pericellular matrix anchored to the plasma membrane (8). In order to achieve osmotic balance with their saline environment, they synthesize and store high concentrations of glycerol in their cytoplasm as an osmolyte (9).

Dunaliella species have been explored in a number of biotechnological applications due to their ability to thrive in harsh environments that suppress the growth of other species (10). Using only the widely available inputs of sunlight, seawater, and CO_2, *Dunaliella* is capable of robust growth and can be harnessed to produce various useful products without competing for valuable resources (e.g., fertile soil and freshwater) necessary for other more traditional forms of agriculture. These features make *Dunaliella* an appealing platform for the sustainable production of many important bioproducts, including glycerol and carotenoids (10–12).

Reviewers: U.W.G., Washington University in St Louis College of Arts and Sciences; and C.C.P., NIH.

The authors declare no competing interest.

[1]L.D. and S.D.G. contributed equally to this work.

[2]To whom correspondence may be addressed. Email: gallaher@berkeley.edu or sabeeha@berkeley.edu.

[3]Present address: Illumina Artificial Intelligence Laboratory, Illumina, Inc., Foster City, CA 94404.

[4]Present address: Department of Biochemistry and Molecular Biology, Plant Research Laboratory, Michigan State University, East Lansing, MI 48824.

This article contains supporting information online at https://www.pnas.org/lookup/suppl/doi:10.1073/pnas.2305495120/-/DCSupplemental.

Published July 17, 2023.

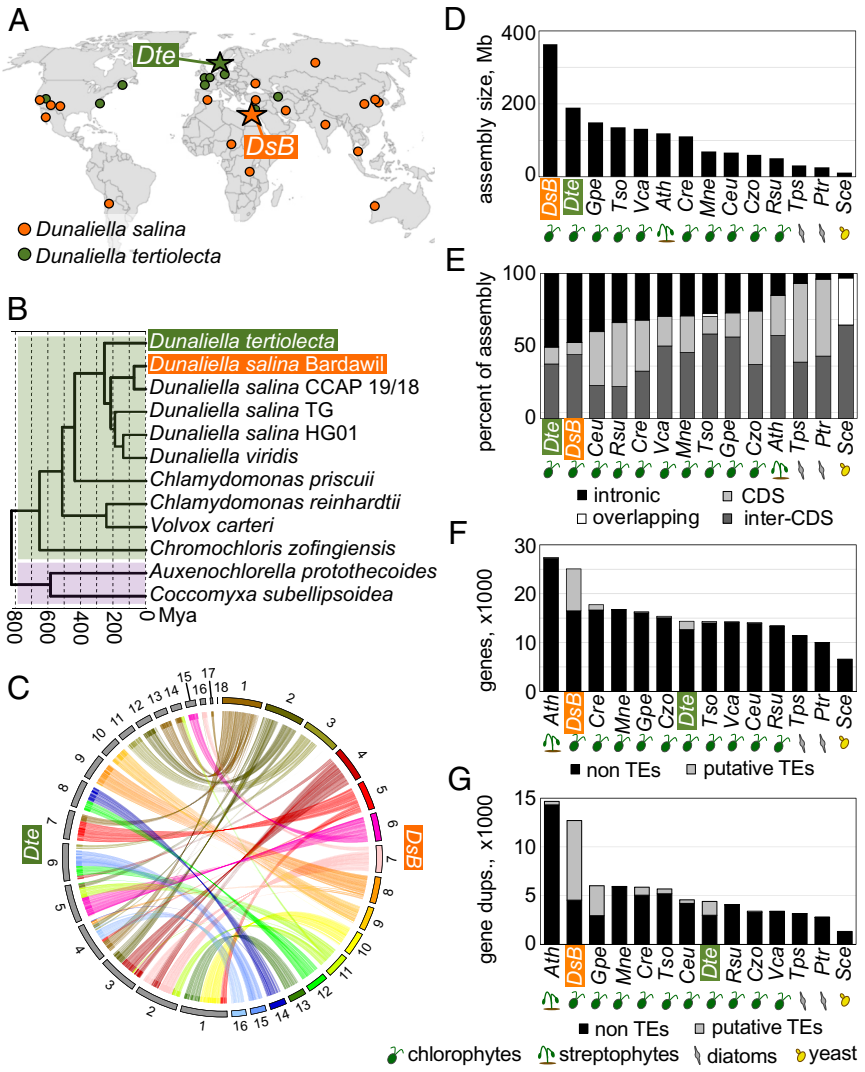

Fig. 1. *Dunaliella salina* Bardawil and *D. tertiolecta* have large genomes due to large introns and transposable element expansion. (*A*) The geographic origins of many field isolates of *D. salina* (orange) and *D. tertiolecta* (green) are shown. The strains used in this work, *D. tertiolecta* UTEX LB 999 and *D. salina* Bardawil UTEX LB 2538, are indicated by stars. (*B*) A chronogram shows the divergence times between several isolates of *Dunaliella* and other green algae from class Chlorophyceae (green) and Trebouxiophyceae (lavender). The chronogram is based on the concatenated polypeptide sequences of 104 universal single-copy orthologs (USCOs) shared among all 12 species (*Methods*). (*C*) A circos plot shows the synteny between the 16 chromosomes of *D. salina* Bardawil (right half) and the 18 scaffolds of *D. tertiolecta* (left half), and demonstrates the 1:1 relationship between the two assemblies. (*D*) The size of each genome assembly is presented as a bar plot arranged from largest to smallest. A three-letter code identifies each species as follows: *DsB* = *D. salina* Bardawil, *Dte* = *D. tertiolecta*, *Gpe* = *Gonium pectorale*, *Tso* = *Tetrabaena socialis*, *Vca* = *Volvox carteri*, *Ath* = *Arabidopsis thaliana*, *Cre* = *C. reinhardtii*, *Mne* = *Monoraphidium neglectum*, *Ceu* = *Chlamydomonas eustigma*, *Czo* = *Chromochloris zofingiensis*, *Rsu* = *Raphidocelis subcapitata*, *Tps* = *Thalassiosira pseudonana*, *Ptr* = *Phaeodactylum tricornutum*, and *Sce* = *Saccharomyces cerevisiae*. Species identifiers are decorated with a symbol indicating their phylogenetic lineage according to the table at the bottom-right of the figure. (*E*) For the same species, the percentage of each genome assembly that is protein-coding sequence (CDS), intronic, inter-CDS sequence, or some overlap of CDS and/or intronic is indicated by the color-coded fractions of each bar. Species are arranged from the most to the least intronic. Further analysis of the contributions of introns is detailed in *SI Appendix*, Fig. S3. (*F*) For the same species, the total number of annotated protein-coding genes is presented as a bar plot arranged from most to fewest genes. (*G*) Gene duplications for each species were computationally predicted. The number of gene duplications is plotted as a bar plot arranged in decreasing order. The fraction of annotated genes that are predicted to be transposable elements (TEs) are indicated in gray in panels *F* and *G*.

In this work, we focused on two species of *Dunaliella* that live in radically different environments. The first, *D. tertiolecta*, is commonly found in coastal sea waters worldwide (Fig. 1*A*). It is under development for the production of biofuels because it is capable of accumulating large quantities of neutral lipids that can be refined into biodiesel (11). The second species, *D. salina*, is found in hypersaline environments and salt flats. *D. salina* has many of the same characteristics as *D. tertiolecta*, making it an attractive platform for producing bioproducts. For example, the strain of *D. salina* used in this work is the richest natural source of β-carotene, a highly valuable commercial product (10, 13). Having been isolated from a salt pond near the Bardawil Lagoon, this strain is sometimes called *D. bardawil* and will be referred to as *D. salina* Bardawil throughout this work.

Much like their ability to tolerate extremes of temperature and salt, *Dunaliella* species are exceptional at maintaining Fe homeostasis in environments where the bioavailable Fe is growth limiting to other species. Tolerance to high salt and low Fe bioavailability may have coevolved since extreme saline conditions drastically reduce Fe solubility. Remarkably, these algae are able to maintain photosynthetic capacity under polyextreme conditions without a major impact on growth (14), suggesting the existence of unique functionality not found in other photosynthetic organisms. Here, we have employed a multiomics strategy to elucidate how *D. tertiolecta* and *D. salina* Bardawil manage environmental extremes, especially low Fe. As a foundation for this work, we generated high-quality, chromosome-scale genome assemblies and transcriptomes for both species. With transcriptomics and proteomics

analyses, we identified the key proteins that these species rely on for their exceptional ability to thrive in low Fe and other harsh conditions. We elucidated the mechanisms that *Dunaliella* deploys for maintaining growth in low Fe and related these to strategies used by other plants and by diatoms. The annotated genomes coupled with transcriptomic and proteomic data that accompany this work will provide a solid foundation to the community for continuing discoveries on extremophilic algae and beyond.

Results

Genomics, Transcriptomics, and Proteomics of *D. tertiolecta* and *D. salina* Bardawil Reveal Keys Genes Important for Fe Homeostasis. To elucidate how these *Dunaliella* species evolved to manage their Fe quota (*SI Appendix*, Fig. S1), we chose a systems biology approach, a strategy best employed when a high-quality genome assembly and a complete set of gene annotations can provide a solid foundation for the analysis. Using a combination of complementary techniques, we generated a chromosome-complete assembly (16 nuclear chromosomes plus a plastome and a mitogenome) for *D. salina* Bardawil and a near chromosome-complete assembly (18 scaffolds plus a plastome and a mitogenome) for *D. tertiolecta* (Fig. 1 and *SI Appendix*, Table S1 and *Text*) that represent a significant improvement in quality over a previously reported draft nuclear genome for *D. salina* (15) and two de novo transcriptomes generated from *D. tertiolecta* (16, 17) (*SI Appendix*, *Text* and Table S2). We found that these two extremophilic *Dunaliella* species, which we estimate diverged ~253 Mya (Fig. 1*B*), have haploid nuclear genomes that are exceptionally large relative to other mesophilic chlorophycean algae (Fig. 1*D* and *SI Appendix*, *Text*). For the *Dunaliella* genome assemblies presented here, we attribute their considerable size to a combination of being rich in transposable elements (TEs) and repetitive sequences (Fig. 1 *F* and *G* and *SI Appendix*, *Text*, Fig. S2, and Table S3) and having very large introns (Fig. 1*E* and *SI Appendix*, *Text* and Fig. S3). The more extremophilic species, *D. salina* Bardawil, has a significantly larger genome, more protein-coding genes, more TEs, and more gene duplications than *D. tertiolecta* (Fig. 1 *D*–*G* and *SI Appendix*, Table S4).

Next, we performed transcriptomics and proteomics on both species grown in defined media with and without added Fe to identify the key Fe-homeostasis genes (Fig. 2 and Dataset S1). For both species, growth in media ±Fe had no effect on the growth rate, and

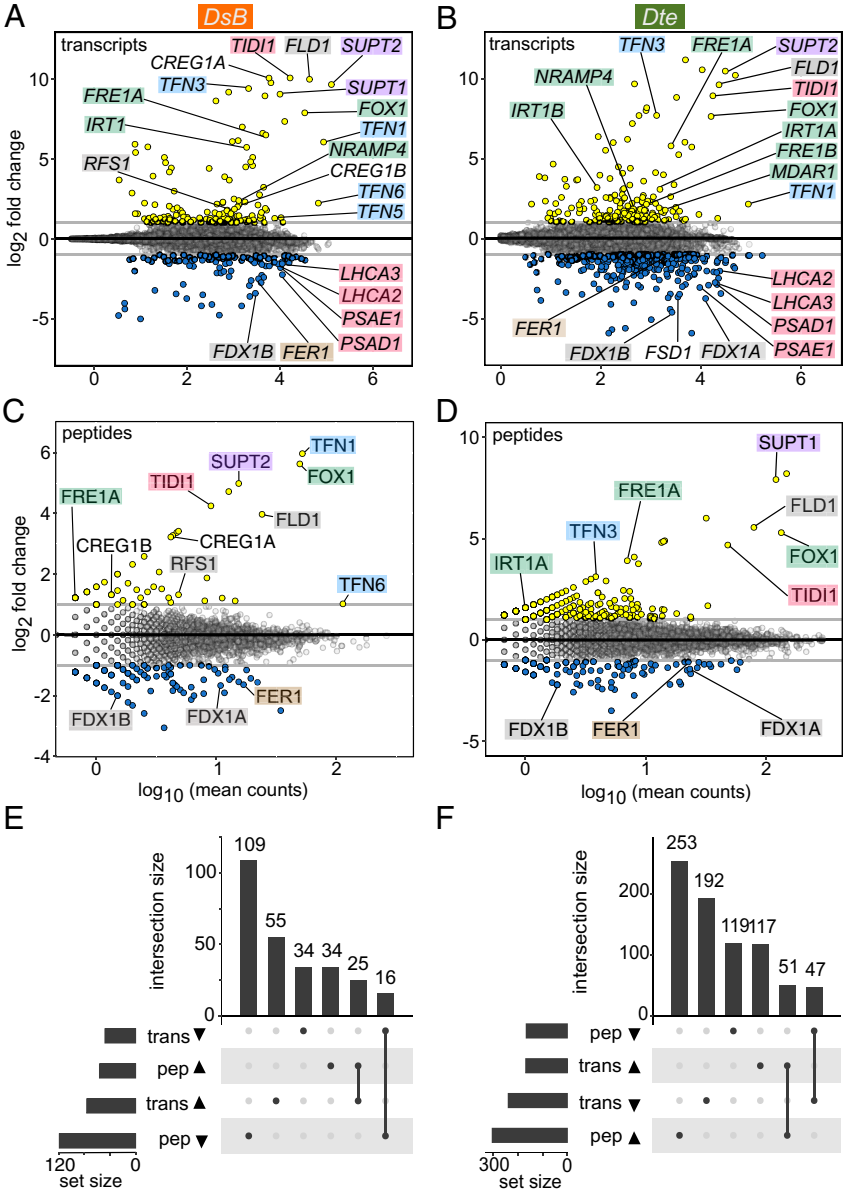

Fig. 2. Dynamic gene expression in *D. salina* Bardawil and *D. tertiolecta* in response to –Fe. Cultures of *D. salina* Bardawil and *D. tertiolecta* were grown in media ±Fe and gene expression was analyzed via transcriptomics and proteomics. (*A*) An MA plot demonstrates DEGs for *D. salina* Bardawil in –Fe relative to +Fe: up-regulated in yellow and down-regulated in blue. A $\log_2$ foldchange = 1 threshold is indicated by horizontal gray lines. Select DEGs are labeled in the figure with the following color scheme: green = reductive Fe uptake proteins, blue = transferrins, lavender = siderophore-uptake proteins, pink = photosystem components, brown = ferritin, and gray = Fe-sparing related. (*B*) The same analysis presented in panel A was performed here on *D. tertiolecta*. (*C*) MA plot of differentially detected spectral counts for proteins from *D. salina* Bardawil cultures grown without Fe vs. with Fe. Proteins were considered up (yellow) or down (blue) if the $\log_2$ fold change of spectral counts plus a pseudocount of 1 was >1. Select differentially detected proteins are labeled using the same color scheme as in panel *A* and *B*. (*D*) The same analysis was performed here on *D. tertiolecta*. (*E*) An upset plot demonstrates the overlap between differentially detected transcripts and differentially detected proteins for *D. salina* Bardawil in response to –Fe. (*F*) The same analysis was performed here for *D. tertiolecta*.

cultures appeared healthy and dark green (*SI Appendix*, Fig. S1). While the vast majority of *D. salina* Bardawil's ~25,000 genes were minimally affected by the change in available Fe, the expression of a few hundred genes was radically altered, increasing by as much as 10^3-fold in the –Fe samples. In *D. salina* Bardawil, we identified 80 up-regulated and 50 down-regulated (Fig. 2*A*) differentially expressed genes (DEGs). In *D. tertiolecta*, which was more significantly impacted by –Fe growth, we identified 169 up-regulated and 239 down-regulated DEGs (Fig. 2*B*). Most of these Fe-regulated genes had orthologs in both species, which suggests that *Dunaliella*'s Fe homeostasis mechanisms predate the split of these two species ~253 Mya. Included in the group of genes that are highly up-regulated in –Fe are all the components of a reductive Fe-uptake pathway, such as a Ferroxidase (FOX1) and a Ferric reductase (FRE1A) (*SI Appendix*, Fig. S4). The down-regulated genes included components of the photosynthetic apparatus, and the Fe-storage protein, Ferritin (FER1). In the following sections, we present some of the more unexpected discoveries.

There Has Been a Major Expansion of Fe-Binding Transferrin Family Proteins in *Dunaliella*. When we examined the most highly Fe-regulated genes, we found a large number of previously unknown Transferrin-family (Tf) proteins in both *Dunaliella* species. Tf proteins were first identified in mammals as soluble glycoproteins with two Fe^{+3} ion-binding domains that mediate Fe transport into cells by binding a cell surface receptor and subsequent endocytosis (18). While two Tf-family proteins had been identified in *D. tertiolecta* previously (19, 20), we discovered a much larger expansion of Tf-encoding genes in the *Dunaliella* lineage (*SI Appendix*, Fig. S5), resulting in seven Tf-encoding genes in *D. tertiolecta* and six in *D. salina* Bardawil (Fig. 3*A*). Estimation of the divergence times of the different *Dunaliella* Tf proteins (*SI Appendix*, Fig. S5) indicates that Tf gene expansion in the *Dunaliella* lineage occurred at multiple points after the Neoproterozoic oxygenation event. This period was marked by increased levels of O_2 leading to oxidation of environmental Fe, factors that would place a premium on ferric iron-uptake mechanisms.

The classically defined Tf proteins in other species predominantly have one or two Tf domains. In contrast, we found that the Tf proteins expressed in *Dunaliella* were highly variable in size, with as few as one and as many as ten Tf motifs (Fig. 3*A*). All 13 *Dunaliella* proteins were predicted to have a transmembrane domain as well as a signal peptide and one or more glycosylation sites, supporting a role for the Tf proteins on the cell surface with their Fe-binding domains extending outside the cell. Thus, it is likely that the *Dunaliella* Tf proteins have the dual function of Fe binding and internalization, which contrasts with the soluble Tf proteins of metazoans that must bind a receptor for cellular Fe uptake. Despite these differences relative to the classically defined Tfs of metazoans, the conservation of Fe- and anion-binding residues (*SI Appendix*, Table S5) and the predicted structures of the *Dunaliella* Tf domains validates that these are true Tf proteins (*SI Appendix*, Fig. S6).

Transcriptomic and proteomic analyses of the *Dunaliella* Tfs show very high levels of expression and protein abundance for many of the Tfs. The most abundant ones are dramatically up-regulated in the low Fe condition (Fig. 3*A*), suggesting an important role for these Tf proteins in Fe uptake. In a survey of all 44 *Dunaliella* Tf domains (from 13 Tf proteins), we observed that domains generally either retain all Fe-binding amino acid residues (21) (shown as

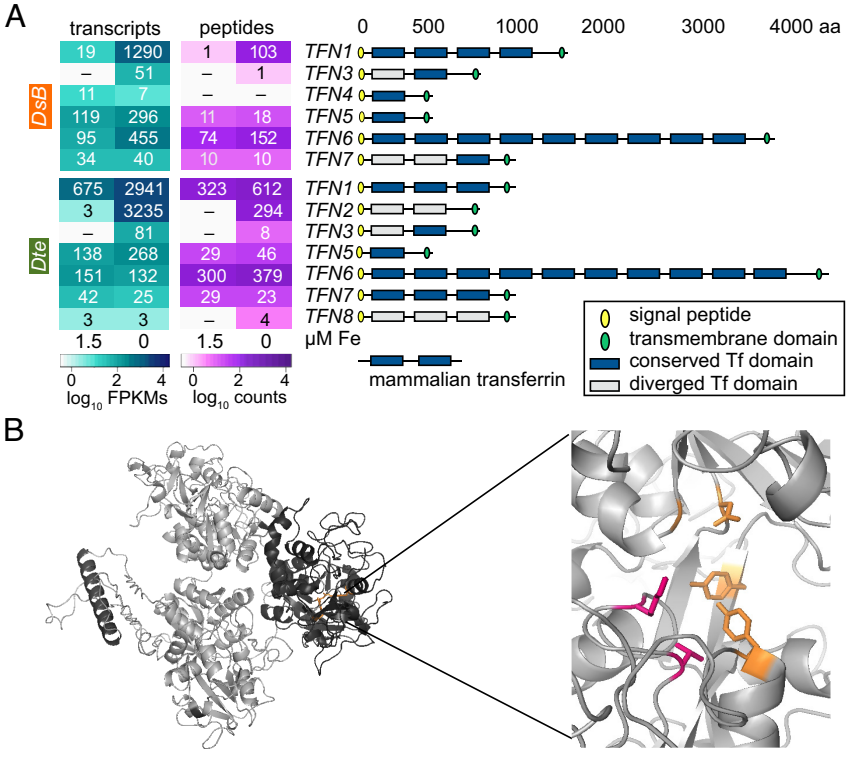

Fig. 3. Expansion of Transferrin-encoding genes in *Dunaliella* helps manage Fe scarcity. (*A*) On the *Left*, a heat map of transcript abundance estimates as $\log_{10}$-transformed FPKMs and protein abundance estimates as $\log_{10}$-transformed spectral counts are presented for the six transferrins of *D. salina* Bardawil and the seven transferrins of *D. tertiolecta* from cultures grown ±Fe, as indicated. To the *Right*, a cartoon demonstrates significant features of each predicted protein as described by the legend. A Tf domain was considered conserved (dark blue) if it retains five key residues involved in Fe and anion binding, or diverged (gray) if not. A protein model of a canonical two-domain, soluble human Tf is included for reference. (*B*) Structure prediction of *D. tertiolecta* TFN1 shows a three-domain protein. An inset panel magnifies residues that are expected to be involved in Fe binding (G80, Y110, Y249, and N330 in orange) and anion binding (T148 and K152 in pink). See *SI Appendix*, Table S5 for details on conservation of Fe- and anion-binding residues.

"conserved" dark blue boxes in Fig. 3*A*) or retain few of the conserved residues (shown as "diverged" gray boxes). The Tf proteins that have retained most or all of the Fe-binding residues were also the most highly expressed in response to low Fe. Combined with the lack of Fe-responsive expression, the divergent Tf proteins, such as *D. tertiolecta* TFN8, may be becoming pseudogenes or have developed a different, novel function.

A Family of Proteins of Unknown Function May Mediate Siderophore–Fe Uptake in *Dunaliella*. In a previous analysis of *D. tertiolecta* (incorrectly reported in that work as *D. salina*), an unknown plasma membrane-bound glycoprotein was isolated from Fe-limited cells (22). This protein was only detected under Fe limitation conditions and was physically associated with FOX1, TFN1, and TFN2. At that time, the authors were unable to find similarity between this glycoprotein and any known proteins and named it "p130B" based on its 130-kDa molecular weight. In the present survey, we identified the *D. tertiolecta* p130B-encoding gene as one of a family of genes with multiple homologs in both *Dunaliella* species: two in *D. salina* Bardawil and three in *D. tertiolecta*.

Transcription of all five of these *Dunaliella* p130B-like genes, which we have named *SUPT1–SUPT4* (see below), was strongly up-regulated in response to Fe limitation (Fig. 4*A*). Protein abundances were similarly increased in the –Fe condition for all except *D. salina* Bardawil SUPT1, an observation which we attribute to a recent nonsense mutation in the corresponding gene (*SI Appendix*, *Text* and Fig. S7). Similar to the Tfs, all five of the *SUPT* genes were predicted to encode a signal peptide, a transmembrane helix at the C terminus, and one or more glycosylation sites (Fig. 4*A*), which is consistent with a role for these proteins on the cell surface. Structure prediction of SUPT1 from *D. tertiolecta* revealed two adjacent seven-bladed β-propeller domains and a transmembrane domain, which is consistent with a cell-surface-located, ligand-binding protein (Fig. 4*C*).

To identify the role of SUPT-family proteins in coping with Fe-deficiency stress, we looked for similar proteins with a known function. The *Dunaliella* SUPT proteins share similarity with metazoan Follistatin, which is a cell surface–bound, ligand-binding glycoprotein. More importantly, the SUPTs share similarity with iron starvation–induced protein 1 (ISIP1) in diatoms such as *Phaeodactylum tricornutum* (Fig. 4*B*). ISIP1 mediates siderophore–Fe uptake via endocytosis (23). Like *D. tertiolecta* SUPT1, we predict that ISIP1 in *P. tricornutum* has a seven-bladed β-propeller structure. The similarities in sequence and predicted structure hint that ISIP1 and SUPT1 may share a function in siderophore–Fe uptake. In support of this hypothesis, *D. salina* Bardawil can utilize siderophore-bound Fe from both microbial siderophores and synthetic chelates (24), but a mechanism for this uptake was not identified until this work. We found no evidence for an endogenous siderophore biosynthetic pathway in either *Dunaliella* species, which suggests that like diatoms, *Dunaliella* relies on nearby organisms to produce and secrete the siderophores that ultimately bind the SUPT proteins (*SI Appendix*, *Text*).

In summary, all five *Dunaliella SUPT* genes are up-regulated in response to low Fe, encode cell-surface proteins with a structure commonly found in ligand-binding proteins, and have sequence and structural similarity to siderophore–Fe-importing proteins in diatoms. From these observations, we propose that the SUPT family of proteins functions as the previously unknown mediator of siderophore-bound-Fe uptake in *Dunaliella*. Based on this function, we have assigned the name *SUPT* to this family of genes.

Quantitative Proteomics Elucidates the Fe-Sparing Benefit of Replacing Ferredoxin with Flavodoxin in *Dunaliella*. While increased assimilation of an essential mineral nutrient, such as Fe or Cu, is a first line of defense in the face of deficiency, elemental sparing is another (25–27). During sparing, the cell replaces a protein that is dependent on the missing element with an isofunctional protein that does not (28). Typically, this mechanism operates on abundant

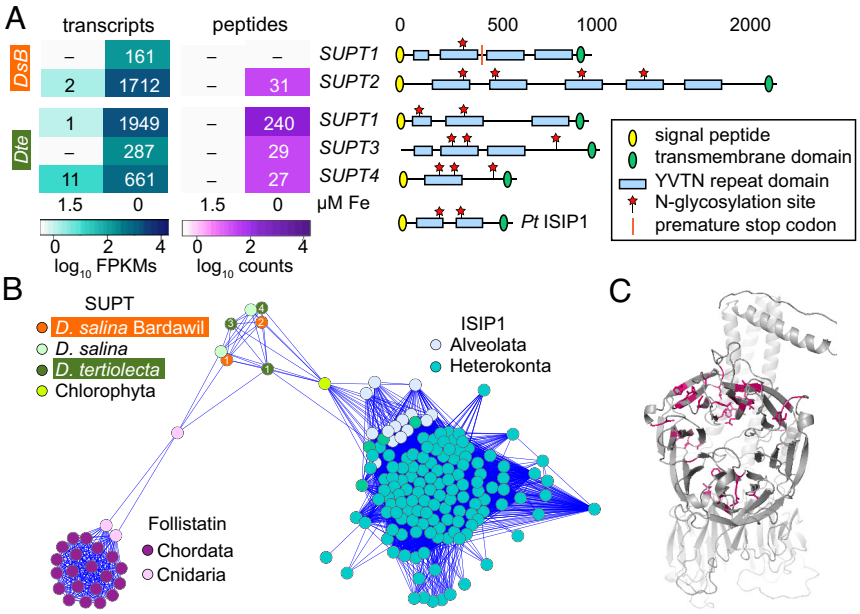

Fig. 4. Proteins in the p130B family may facilitate siderophore–Fe uptake in *Dunaliella* species. (*A*) Heat maps for transcript and protein abundance levels of *SUPT1–SUPT4* in *D. salina* Bardawil and *D. tertiolecta* grown in media ±Fe. To the right of each *SUPT* gene symbol is a cartoon of the predicted protein structure. Predicted features are presented as described in the accompanying legend. A single stop codon in *D. salina* Bardawil *SUPT1* breaks up an otherwise conserved open-reading frame and is indicated here by a red line (*SI Appendix*). (*B*) A protein similarity network of *Dunaliella* SUPT proteins and likely chlorophyte orthologs, ISIP1 proteins from diatoms, and metazoan follistatins. The similarity network was generated using blastp comparison of all-vs-all on over 100 sequences using E-value of 1×10^{-25}. (*C*) The structure of *D. tertiolecta* SUPT1 was predicted to consist of two 7-blade propeller domains, one facing the viewer and the second perpendicular to it, and an alpha helix transmembrane domain. The 50 amino acids that are conserved among all *Dunaliella* SUPT proteins and their *Chlamydomonas schloesseri* orthologs are marked in pink.

proteins leading to significant reduction in the demand for the missing element. The replacement of FeS-containing ferredoxin, which functions in various anaerobic bioenergetic pathways, by flavin-containing flavodoxin under poor iron nutrition was noted decades ago in *Clostridium spp.* (29, 30). This switch also occurs in the photosynthetic apparatus of cyanobacteria (31, 32), where the dominance of either protein is a classic biomarker for the iron status of the ocean (33). The operation of this ferredoxin/flavodoxin switch is not well investigated in eukaryotic algae. In fact, the flavodoxin gene is absent in plants and in *Chlamydomonas* species (34), leading to the dogma that this sparing mechanism was not retained after evolution of the chloroplast from the endosymbiont. Nevertheless, analysis of the *Dunaliella* genomes revealed *FLD1,* which encodes a type 2 flavodoxin (35), and a pair of paralogous ferredoxin-encoding genes (*FDX1A* and *FDX1B*) in both *D. tertiolecta* and *D. salina* Bardawil. The *FDX1* genes are highly expressed in +Fe, with *FDX1A* being dominant, and dramatically down-regulated in –Fe (Fig. 5*A*), while expression of *FLD1* was counterregulated. Curiously, downregulation of *FDX1A* occurred at the level of transcription in *D. tertiolecta* but at the level of protein abundance in *D. salina* Bardawil (Fig. 5*A*), speaking perhaps to independent evolution of the regulatory circuit that controls sparing.

Next, we quantified the benefit of replacing FDX with FLD as an Fe-sparing mechanism for eukaryotic organisms. Replacement of FDX1A with FLD1 allows the cell to free up two Fe atoms per molecule of FDX1A. To evaluate the impact of replacement on a per-cell basis, we quantified the two proteins in *D. salina* Bardawil by selected reaction monitoring (SRM) proteomics (37). FDX1A, at an abundance of 5.1×10^7 molecules/cell, decreased by 23-fold in the low Fe condition to 2.2×10^6 molecules/cell, while FLD1 increased 106-fold to an abundance of 1.5×10^7 molecules/cell (Fig. 5*B*). Thus, a *D. salina* Bardawil cell can free up 1×10^8 atoms of Fe solely by replacing FDX1A with FLD1. Concurrently, the Fe quota of the algal cell decreased threefold from 1.5 to 0.49×10^9 atoms per cell in +Fe vs. –Fe, which translates to an Fe allocation of 6% to FDX1A in the Fe-replete situation vs. only 0.9% in low Fe.

The metabolic cost of this switch [besides perhaps reduced electron transfer rates by the substitute protein (38)] is a substantial draw on the flavin cofactor pool (39). Among the DEGs, we noted increased expression of key enzymes in the flavin biosynthetic pathway of *D. salina* Bardawil (Fig. 5*C*), including the dual-function RIBBA1 protein, which initiates the flavin biosynthesis pathway, and RFS1, which converts 6,7-dimethyl-8- (1-D-ribityl) lumazine to riboflavin. When we quantified the levels of three flavin end products of the pathway, riboflavin, FMN, and FAD (Fig. 5 *C*, *Inset*), we noted that FMN, the flavin cofactor in FLD1, is the most dramatically increased: over sixfold in the –Fe vs. +Fe condition. Taken together, these results show a coordinated effort by the cell to replace FDX1 and its 2Fe2S cluster with FLD1 and FMN when the available Fe is low.

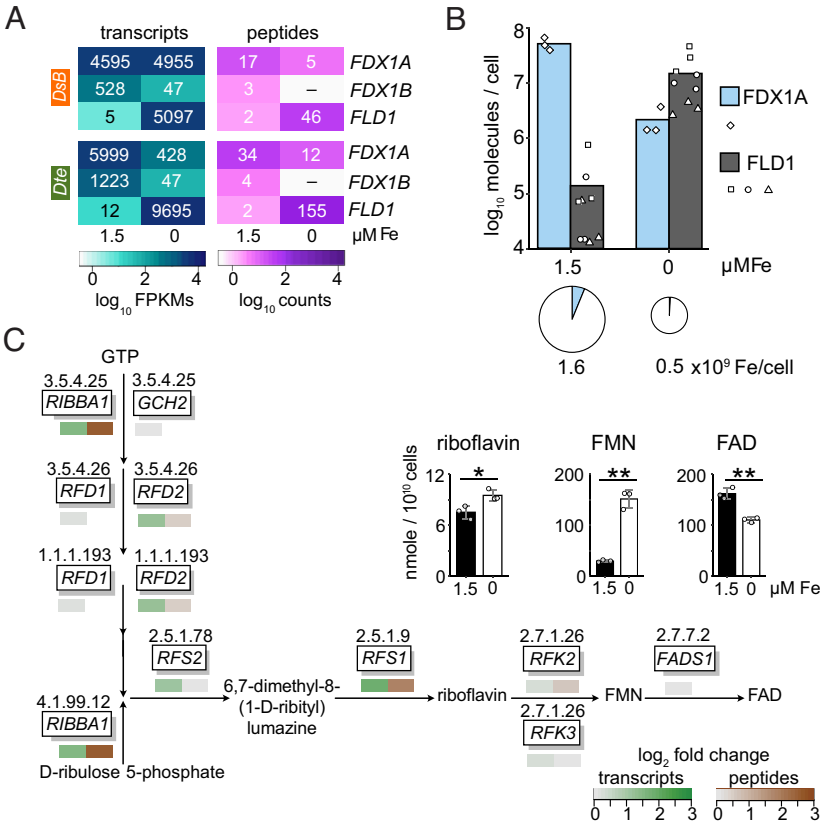

Fig. 5. *Dunaliella* replaces ferredoxin with flavodoxin as an Fe-sparing mechanism. (*A*) Transcript and protein abundances for *FDX1A*, *FDX1B*, and *FLD1* are presented for *D. tertiolecta* and *D. salina* Bardawil cultures grown in media ±Fe. (*B*) Selected reaction monitoring (SRM) proteomics was used to quantify the number of FDX1A (light blue) and FLD1 (dark gray) molecules in *D. salina* Bardawil cells grown in media ±Fe. The resulting counts per cell were $\log_{10}$ transformed and plotted as the mean number per cell (*Top*). Triplicate determinations of one peptide for FDX1A ($n = 3$) and three peptides for FLD1 ($n = 9$) are overlaid as white symbols. Below, The total cellular Fe content was quantified by inductively coupled plasma mass spectrometry and is indicated by the relative size of each pie. The proportion of Fe atoms expected to be bound to FDX1A, which is shown by the light blue pie slice, was calculated assuming two Fe atoms per molecule of FDX1A and that only the metalated protein is stable (36). (*C*) Components of the flavin biosynthesis pathway are presented along with their products. Heat maps showing the fold change in transcripts (green) and proteins (brown) in –Fe relative to +Fe are shown under each gene. Genes symbols are as follows: *RIBBA1* = riboflavin biosynthesis, *GCH2* = GTP cyclohydrolase type II, *RFD1/RFD2* = riboflavin metabolism-associated deaminase, *RFS1/RFS2* = riboflavin synthase, *RFK2/3* = riboflavin kinase, *FADS1* = FAD synthase. The quantity of three key metabolites, riboflavin, flavin mononucleotide (FMN), and FAD, were measured from cultures grown ±Fe ($n = 3$). Statistical significance is indicated as follows: ns = $P \geq 0.05$, * = $P < 0.05$, ** = $P < 0.005$.

Downregulation of Photosystem I (PSI) in Favor of PSII Allows Maintenance of Photosynthesis with a Lower Fe Quota. Many of the key components of the photosynthetic apparatus require Fe to function. Since obligately photoautotrophic organisms like *Dunaliella* depend on photosynthesis for life, insufficient Fe can be fatal without countermeasures. About half the Fe in the photosynthetic apparatus is found in PSI due to the three 4Fe-4S clusters in each PSI complex (40). A common acclimation strategy in cyanobacteria is a change in the ratio of PSI to PSII in low Fe to favor PSII with its much lower Fe requirement (41). We annotated PSI and PSII components in both *D. tertiolecta* and *D. salina* Bardawil and quantified the expression of these genes ±Fe. All PS genes were very highly expressed, nearly 10^5 FPKMs for *PSBR1* in *D. tertiolecta*, and all were down-regulated in low Fe (*SI Appendix*, Fig. S8). However, not all PS components were down-regulated equally. In *D. tertiolecta*, a PSI component, *PSAE1*, was down-regulated 8.7-fold, while a PSII component, *PSBY1,* was down-regulated only 1.4-fold. When the downregulation of either PSI or PSII components was averaged, the PSI components were significantly more down-regulated (Fig. 6*A*), consistent with prioritization of PSII over PSI. In *D. salina* Bardawil, the mean $\log_2$-transformed fold decrease was 1.5 for PSI vs. 0.8 for PSII. While the difference was significant in both species, it was more pronounced in *D. tertiolecta*: 2.5 vs. 1.0.

In the Viridiplantae, multiple PSI-associated light-harvesting complex proteins (LHCAs) act as photon-capturing antennae for PSI. In previous work, an LHCA3-like protein called TIDI1, expressed exclusively under Fe-starvation conditions, had been discovered in *D. tertiolecta* (reported in that work as *D. salina*) and purported to be an accessory antenna to PSI (14). Indeed, *TIDI1* is highly up-regulated in both *Dunaliella* species, in contrast to canonical *LHCA3* (Fig. 6*C*). *TIDI1* is not present in *Chl. reinhardtii* (reference alga in the green lineage) or in land plants. However, we discovered TIDI1-encoding genes in the genomes of four other green algae from the order Sphaeropleales: *Chromochloris zofingiensis*, *Flechtneria rotunda*, *Tetradesmus deserticola*, and *Scenedesmus* sp. NREL 46B-D3. Since *Dunaliella* belongs in order Chlamydomonadales, this suggests that *TIDI1* first arose over 651 Mya (Fig. 1*B*) or else is the result of horizontal gene transfer between species in the Chlamydomonadales and Sphaeropleales lineages. A protein similarity network (Fig. 6*B*) demonstrates that the chlorophycean TIDI1 proteins are related but distinct from the LHCA3 proteins of chlorophytes and streptophytes.

To explore the relationship between TIDI1 and LHCA3 further, we computationally predicted structures for both proteins and found that while they are nearly identical, two features distinguish them (Fig. 6*E*). First, the TIDI1 proteins have a longer, proline-rich N-terminal extension relative to LHCA3. Second, TIDI1 proteins have an additional 10 to 12 amino acids in the loop between alpha helices B and C (Fig. 6 *D* and *E*). In all the TIDI1 proteins we identified, we found five highly conserved residues in the interhelix loop arranged as PFxGxxPF. We propose that this pattern could be used as a marker for the identification of TIDI1 as a distinct protein from LHCA3 in other organisms as their genomes are sequenced. In the predicted structure, the orientation of the interhelix loop places two bulky, hydrophobic Phe residues outward facing (Fig. 6*E*), which could suggest a TIDI1-specific docking site for binding to the PSI complex.

***Dunaliella* Shares Some Fe-Related Proteins with Plants and Others with Diatoms.** There is rich literature on components of Fe homeostasis in the green lineage and diatoms because of the high abundance of Fe-containing proteins in the photosynthetic apparatus (42–44). For a phylogenomic profile of Fe-homeostasis proteins, we identified orthologs of Fe-related proteins from three chlorophytes (*D. salina* Bardawil, *D. tertiolecta*, *Chl. reinhardtii*), two streptophytes (*Arabidopsis thaliana* and *Oryza sativa*), and three diatoms (*Fragilariopsis cylindrus, P. tricornutum*, and *Thalassiosira oceanica*) (Fig. 7).

Among these eight species, TIDI1 and the expanded family of Tf proteins are unique to *D. tertiolecta* and *D. salina* Bardawil. Other responses to poor Fe nutrition are conserved between *Dunaliella* and the other members of the green lineage, such as increased expression of monodehydroascorbate reductase 1 (MDAR1) and natural resistance-associated macrophage protein 4 (NRAMP4). In contrast, FLD1 and the SUPT/ISIP1-family proteins are shared only with diatoms, which lie on a different branch of the tree of life, separated from *Dunaliella* by approximately 1.5 billion years of evolution (46).

Recently, the Fe-uptake protein, ISIP2a, was identified in diatoms undergoing Fe insufficiency (47). This protein is sometimes described as phytotransferrin. While this protein may share a common function with the canonical Tf proteins from *Dunaliella*, metazoans, and some land plants, it is distinctly different in terms of amino acid similarity and predicted structure (*SI Appendix*,

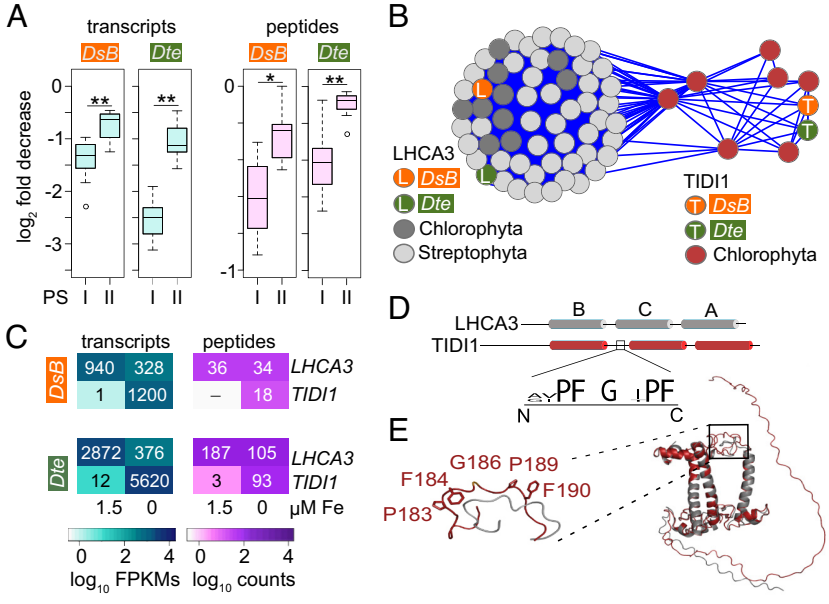

Fig. 6. *Dunaliella* remodels its photosystem in response to low Fe, including upregulation of TIDI1. *Dunaliella* species can alter the composition of their photosynthetic machinery to acclimate to low Fe. (*A*) On the *Left*, box plots of the $\log_2$ fold change decrease in the –Fe vs. +Fe condition for transcripts encoding components of PSI (n = 9) and PSII (n = 7) for *D. salina* Bardawil and *D. tertiolecta*. On the *Right*, the same analysis for PSI (n = 7) and PSII (n = 7) proteins detected by at least two spectral counts is shown. Statistical significance is indicated as follows: ns = $P \geq 0.05$, * = $P < 0.05$, ** = $P < 0.005$. See also *SI Appendix*, Fig. S7. (*B*) A protein sequence similarity network of LHCA3 and TIDI1 proteins from chlorophytes and streptophytes was generated using an E-value of 1×10^{-78}. (*C*) Labeled heat maps of transcript and protein abundance for the products of the *LHCA3* and *TIDI1* genes in *D. salina* Bardawil and *D. tertiolecta* grown in media ±Fe. (*D*) A cartoon depicts the three alpha helix structure shared by LHCA3 and TIDI1. Below, a logo plot of the conserved amino acids in a loop between alpha helices B and C that is present in TIDI1 but not LHCA3. (*E*) Predicted three-dimensional structures for *D. tertiolecta* LHCA3 (gray) and TIDI1 (red) are overlaid. The black box highlights the location of the 10 amino acid TIDI1-specific loop and the positions of the most conserved residues.

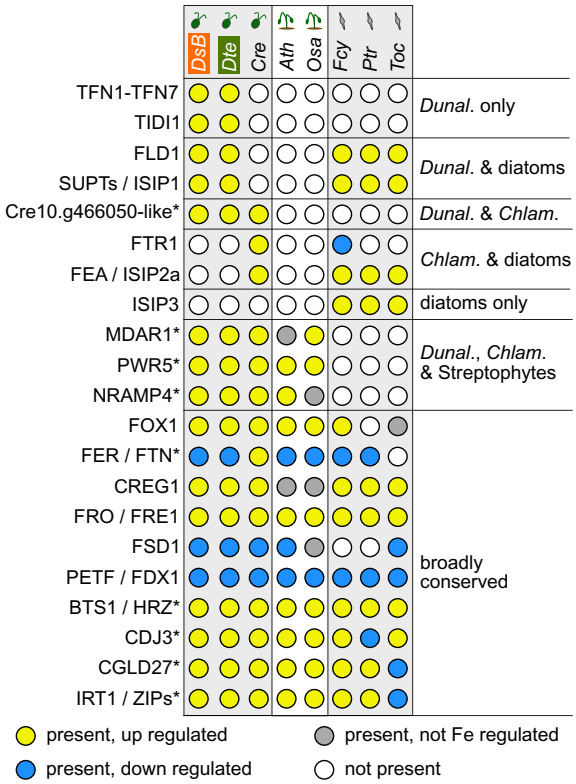

Fig. 7. Some Fe-related proteins are conserved among eight photosynthetic species, others are not. Fe-related proteins that were identified in this work and Urzica et al. 2012 (45) were evaluated to identify homologous proteins in eight species of chlorophytes, streptophytes, and diatoms with RNA sequencing (RNA-Seq) expression data from experiments performed in low and normal Fe. A threshold $|\log_2$-transformed fold change$| > 0.3$ was used to define upregulation and downregulation. Species are as follows: chlorophytes (*DsB* = *D. salina* Bardawil, *Dte* = *D. tertiolecta*, *Cre* = *Chl. reinhardtii*); streptophytes (*Ath* = *Arabidopsis thaliana*, *Osa* = *Oryza sativa*); and diatoms (*Fcy* = *Fragilariopsis cylindrus*, *Ptr* = *Phaeodactylum tricornutum*, *Toc* = *Thalassiosira oceanica*). Proteins identified as being conserved in the green lineage in ref. 45 are highlighted with an asterisk.

Fig. S6), likely the result of convergent evolution. Here, we group ISIP2a with the *Chl. reinhardtii* FEA proteins to which they are related (Fig. 7).

Last, we note that the two *Dunaliella* species carry orthologs of the *Chl. reinhardtii* gene Cre10.g466050. The protein it encodes has no known function, but its conservation and degree of Fe-regulated expression suggest that this may represent a pioneer protein worthy of further study.

Discussion

Dunaliella's ability to grow in harsh conditions where the bioavailable Fe is so low as to be growth limiting for neighboring species makes it an attractive model for study. When we grew *D. salina* Bardawil and *D. tertiolecta* cultures in media without added Fe, we found that they were not affected in growth rate and were only mildly chlorotic, despite an approximately threefold decrease in internal Fe content (*SI Appendix*, Fig. S1). This is in contrast to other algae and land plants that are growth impacted and severely chlorotic under similar conditions. To understand the molecular mechanisms that allow *Dunaliella* to maintain its growth despite Fe scarcity, we produced transcriptomic and proteomic datasets, coupled with biochemical analyses, which facilitated the identification of dozens of genes that contribute to Fe homeostasis in *Dunaliella*.

Within the green lineage, *Dunaliella* are notable for expressing multiple, broadly derived systems of Fe acquisition proteins. (Fig. 8). We describe this as the "mix-and-match" strategy for Fe uptake. First, the reductive Fe-uptake pathway, common in land plants, green algae, and fungi, is characterized by a high uptake rate but a relatively low affinity for Fe. We observed Fe-dependent expression of the key genes in that pathway, such as *FOX1* and *FRE1A* (Fig. 2). Second, siderophore-mediated Fe uptake, commonly found in bacteria and cyanobacteria, has a high affinity for Fe but a low rate of uptake. We propose that a family of highly expressed *Dunaliella* proteins of unknown function (previously known as p130B, and here called SUPTs) is used by the cell for siderophore-bound Fe uptake (Fig. 4). And third, Tf-mediated Fe uptake, first identified and commonly found in metazoans, is capable of very high affinity and fast binding of Fe but requires the production of large quantities of Tf protein, which is energetically costly. We found that both *Dunaliella* species produce several, multidomain, membrane-bound Tf proteins capable of binding up to 10 atoms of Fe simultaneously (Fig. 3). This major expansion of Tf-encoding genes highlights the importance of this particular strategy for *Dunaliella*. Each of these three different Fe-uptake strategies was first identified in far-flung clades of the tree of

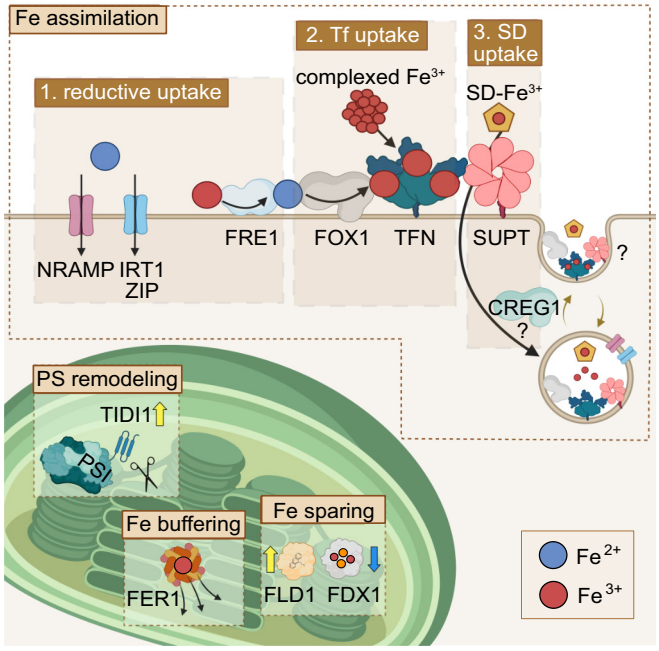

Fig. 8. Summary of Fe-responsive mechanisms in *Dunaliella* species. Increased Fe assimilation in *Dunaliella* is mediated by three mechanisms that allow uptake of all forms of Fe. 1. The reductive mechanism, which includes induction of the FRE1A reductase and nonspecific divalent metal transporters, like iron responsive transporter 1 (IRT1), other Zrt/Irt-like protein (ZIP) family transporters, and NRAMP4. These proteins may also play a role in transporting Fe out of endosomes. 2. Tf-mediated uptake is conferred by a large family of high-affinity Fe^{+3}-binding proteins. A copper-dependent FOX1, which mediates the uptake of Fe^{+2}, may participate in reductive uptake but has also been observed in association with TFN1 (22). 3. Proposed uptake of siderophore-bound Fe via binding to SUPT family proteins. Cellular Repressor of E1A Stimulated Genes 1 (CREG1) is an Fe-regulated protein that may play a regulatory role in Fe uptake. In addition to increased uptake, the Fe quota is maintained by the remodeling of the photosynthetic apparatus, which includes the preferential downregulation of PSI vs. PSII components, and the addition of the accessory antenna protein TIDI1. Additional Fe is made available as needed by release of Fe stored in FER1. Fe sparing occurs by replacing the Fe-rich FDX1A protein with FLD1.

life, so it is interesting to consider how the co-occurrence of all three in one species may give *Dunaliella* a fitness advantage.

While each of these strategies may function independently, it is interesting to consider the alternative where they work in tandem. A previous study identified components of all three Fe-uptake strategies (TFN1, TFN2, FOX1, and SUPT1) forming a supercomplex on the plasma membrane of *Dunaliella* (22). Such a super complex would have the ability to bind Fe in whichever form it is encountered: Fe^{2+}, Fe^{3+}, and siderophore-bound. In this model, *Dunaliella* could channel Fe from all three pathways to Tf as follows: from the redox pathway, through FRE1 and FOX1, through the siderophore pathway via the SUPT proteins, and by direct binding to Tf (Fig. 8). In this way, the relative strengths and weaknesses of the three strategies could combine to confer rapid, high-capacity, high-affinity, Fe uptake of whichever form of Fe is available.

The spongy pericellular matrix that surrounds *Dunaliella* cells may also play a role in Fe acquisition. This glycocalyx-like structure is most likely composed of glycoproteins replete with neuraminic acid residues and can extend to 0.5 μM out from the plasma membrane (8). Saccharides have been shown to increase Fe solubility and consequently Fe uptake in eukaryotic phytoplankton (48). Thus, it may be that the saccharide-rich pericellular matrix increases Fe bioavailability in close proximity to the Fe-uptake proteins described above.

It is striking how these two *Dunaliella* species have Fe-homeostasis genes in common with chlorophytes, streptophytes, diatoms, and cyanobacteria. While much of this is certainly due to shared ancestry, we must also consider the possibility that some of these genes are present in *Dunaliella* as the result of horizontal gene transfer. The *SUPT* genes, which we identified in only a few other chlorophytes, represent an intriguing candidate for further study in this regard.

The high-quality genome assemblies, annotated gene catalogs, and transcriptomics/proteomics datasets that accompany this work should be a vital resource for researchers in a variety of fields. For those engaged in engineering *Dunaliella* species for the production of biofuels and other valuable bioproducts, this work will accelerate those efforts. For those concerned about the role that marine algae can play in climate change mitigation efforts by increasing primary productivity, this work identifies a variety of ways in which algae may maintain robust photosynthetic activity despite living in environments with low available Fe, such as the high-nutrient–low-chlorophyll regions of the ocean. Finally, the proteins of these *Dunaliella* species evolved to remain correctly folded and functional in up to 3 M NaCl. Just as the thermostable polymerase of *Thermus aquaticus* facilitated the development of PCR, the proteins of *Dunaliella* that we have identified may prove to be an important source of highly stable proteins for novel applications in synthetic biology and bioengineering.

Materials and Methods

Strains and Culture Conditions. *D. salina* Bardawil and *D. tertiolecta* were gifts of Uri Pick (The Weizmann Institute of Science, Rehovot, Israel). *D. salina* Bardawil is deposited in the University of Texas-Austin Culture Collection of Algae (UTEX) as *Dunaliella bardawil* LB 2538. *D. tertiolecta* is as UTEX LB 999. The medium composition and growth conditions were as described in ref. 49. Briefly, all culture glassware were washed in 6 N HCl and thoroughly rinsed with Milli-Q water. Standard growth medium contained 1 M NaCl (*D. salina* Bardawil) or 2 M NaCl (*D. tertiolecta*), with or without the addition of 1.5 μM $FeCl_3$, 6 μM EDTA as indicated. Culture flasks were grown on shaking platforms (140 rpm) at 24 °C. Constant light at 50 μE m^{-2} s^{-1} (*D. salina* Bardawil) or 100 μE m^{-2} s^{-1} (*D. tertiolecta*) was provided by cool white fluorescent bulbs (4,100 K) and warm white fluorescent bulbs (3,000 K) in a 2:1 ratio. Cells were counted by the Cellometer automated cell counter (Nexcelom).

Protein Structure Predictions. Protein structure predictions were conducted using ColabFold (50) (https://github.com/sokrypton/ColabFold). Structures were visualized with PyMOL (v1.7.4, available at https://pymol.org/). Logo plots were generated with WebLogo (available at https://weblogo.berkeley.edu/) (51).

Orthology Analysis and Estimation of Gene Duplication Events. Orthological and paralogical relationships between proteins and estimation of gene duplication events were determined by OrthoFinder (v2.5.2, available at https://github.com/davidemms/OrthoFinder) using default parameters (52). The number of gene duplications for each species was determined by filtering the Duplications.tsv output of OrthoFinder to include only instances in which both daughter genes were retained in that species to the present day. A full list of the species used, their version numbers, and their sources is provided in *SI Appendix*, Table S6.

Protein Similarity Networks. Protein similarity networks were generated from an all-vs.-all blastp (53) analysis (pairwise alignment between all pairs of proteins) of sequences in a local sequence database. The networks were created in Cytoscape (v3.4) with the BLAST2SimilarityGraph plug-in and the yFiles Organic layout engine provided with Cytoscape. Protein nodes were connected by edges if the E-value between the two sequences was at least as good as the value indicated in the corresponding figure legend.

Proteomics and SRM Quantification. Total soluble protein was collected in parallel with the RNA-Seq samples described above, tryptic digested, and quantified by mass spectrometry as described previously (54). For SRM quantification of FLD1 and FDX1A, peptides were selected that were readily detectable in other samples and that could be uniquely assigned to their respective protein. Heavy versions of these peptides were synthesized with ^{13}C- and ^{15}N-enriched amino acids to label the terminal K or R. Twofold dilution series of each heavy peptide were added to cellular protein samples and assayed to validate the linear range of detection. The optimal concentration of each heavy peptide was added to biological samples in triplicate and assayed. The ratio of light peptide to the spiked-in quantity of the heavy peptide was then used to calculate the quantity of the light peptide on a per-cell basis. Three peptide sequences were used for FLD1: QYDGLIVGSPTWNTGADEER, WAYSEGEYEHTYSK, and VDKWVAQIR. One peptide sequence was used for FDX1A: VESGTVDQSDQSFLDDDQQGR.

Metabolite Analysis. *D. salina* Bardawil cultures were grown in media ±Fe as described above. On day 3, cells were counted, and 50 mL from each flask was collected by centrifugation at 3,500 × *g* for 5 min and washed three times with 1 M NaCl. Cell pellets were weighed and flash frozen in liquid nitrogen. Metabolites were analyzed as described previously (55).

Statistical Analyses. All *n* numbers represent biological replicates (i.e., samples taken from independent culture flasks). Data in bar graphs are expressed as the mean ± SD. Significance was determined by two-sided Student's *t* test. For boxplots, the center line indicates the median, box limits indicate the upper and lower quartiles, whiskers indicate 1.5× the interquartile range, and points indicate outliers.

Data, Materials, and Software Availability. Custom code for calculating exon and introns sizes from a transcriptome is freely available from GitHub under a GNU General Public License at https://doi.org/10.5281/zenodo.7719065 (56). Genomic sequencing data were submitted to the NCBI Sequence Read Archive (SRA) under BioProject PRJNA914849 for *D. salina* Bardawil (57) and BioProject PRJNA914763 for *D. tertiolecta* (58). Transcriptomic data, assembled genomes, and annotation files were submitted to NCBI Gene Expression Omnibus (GEO) archive under accession GSE222140 for *D. salina* Bardawil (59) and GSE222141 for *D. tertiolecta* (60). Accession codes for all other data not generated as part of

this work are detailed in *SI Appendix*, Table S6. Expression data generated in this work are provided in Dataset S1.

ACKNOWLEDGMENTS. We want to thank Uri Pick and Ute Kraemer for their helpful comments. L.D. was supported by the European Molecular Biology Organization (ALTF 166-2016) and by the United States–Israel Binational Agricultural Research and Development (BARD) Fund, Vaadia-BARD Postdoctoral Fellowship Award FI-531-2015. This work was supported by US Department of Energy (DOE), Office of Science, Office of Basic Energy Sciences Award (DE-FG02-04ER15529). Proteomics analyses were supported by an award (49840) from the Environmental Molecular Sciences Laboratory (grid.436923.9), which is a DOE Office of Science User Facility under contract DE-AC05-76RL01830. The research conducted by C.E.B.-H. at the US Department of Energy Joint Genome Institute (https://ror.org/04xm1d337), a DOE Office of Science User Facility, is supported by the Office of Science of the US Department of Energy operated under Contract No. DE-AC02-05CH11231.

Author affiliations: [a]Department of Chemistry and Biochemistry, University of California, Los Angeles, CA 90095; [b]California Institute for Quantitative Biosciences (QB3), University of California, Berkeley, CA 94720; [c]Department of Human Genetics, University of California, Los Angeles, CA 90095; [d]Environmental Molecular Sciences Laboratory, Pacific Northwest National Laboratory, Richland, WA 99354; [e]Biological Sciences Division, Pacific Northwest National Laboratory, Richland, WA 99354; [f]Institute of Biological Chemistry, Washington State University, Pullman, WA 99163; [g]Department of Energy Joint Genome Institute, Lawrence Berkeley National Laboratory, Berkeley, CA 94720; [h]Molecular Foundry, Lawrence Berkeley National Laboratory, Berkeley, CA 94720; [i]Department of Biochemistry, Purdue Center for Plant Biology, Purdue University, West Lafayette, IN 47907; [j]Department of Plant and Microbial Biology, University of California, Berkeley, CA 94720; and [k]Department of Molecular and Cell Biology, University of California, Berkeley, CA 94720

Author contributions: L.D., S.D.G., and S.S.M. designed the study and directed the experiments; L.D., S.S., and S.R. performed biochemical experiments; S.D.G. and E.B.-D. assembled the genomes; L.D., S.D.G., R.J.C., and C.E.B.-H. annotated the genomes; S.D.G. analyzed the transcriptomics data; S.O.P., T.L.F., and C.D.N. generated and analyzed the proteomics data; R.P.A. and J.H.W. contributed sequencing data; S.D.G. contributed new reagents/analytic tools; L.D. and S.D.G. analyzed the data and made the figures; and L.D., S.D.G., and S.S.M. wrote the paper.

1. C. B. Field, M. J. Behrenfeld, J. T. Randerson, P. Falkowski, Primary production of the biosphere: Integrating terrestrial and oceanic components. *Science* **281**, 237–240 (1998).
2. M. J. Behrenfeld *et al.*, Satellite-detected fluorescence reveals global physiology of ocean phytoplankton. *Biogeosciences* **6**, 779–794 (2009).
3. P. W. Boyd *et al.*, Mesoscale iron enrichment experiments 1993–2005: Synthesis and future directions. *Science* **315**, 612–617 (2007).
4. D. Staiger, Chemical strategies for iron acquisition in plants. *Angew. Chem. Int. Ed* **41**, 2259–2264 (2002).
5. J. A. Imlay, Iron-sulphur clusters and the problem with oxygen. *Mol. Microbiol.* **59**, 1073–1082 (2006).
6. A. Del Cortona *et al.*, Neoproterozoic origin and multiple transitions to macroscopic growth in green seaweeds. *Proc. Natl. Acad. Sci. U.S.A.* **117**, 2551–2559 (2020).
7. A. Ben-Amotz, J. E. W. Polle, D. V. S. Rao, *The Alga Dunaliella: Biodiversity, Physiology, Genomics and Biotechnology*, A. Ben-Amotz, Ed. (CRC Press, ed. 1, 2009), (January 21, 2023).
8. J. E. W. Polle, R. Roth, A. Ben-Amotz, U. Goodenough, Ultrastructure of the green alga *Dunaliella salina* strain CCAP19/18 (Chlorophyta) as investigated by quick-freeze deep-etch electron microscopy. *Algal. Res.* **49**, 101953 (2020).
9. K. Wegmann, Osmotic regulation of photosynthetic glycerol production in *Dunaliella*. *Biochim. Biophys. Acta.* **234**, 317–323 (1971).
10. L. J. Borowitzka, M. A. Borowitzka, Commercial production of Beta-Carotene by *Dunaliella salina* in open ponds. *Bull. Mar. Sci.* **47**, 244–252 (1990).
11. A. Patel, B. Gami, P. Patel, B. Patel, Biodiesel production from microalgae *Dunaliella tertiolecta*: A study on economic feasibility on large-scale cultivation systems. *Biomass Convers. Biorefin.* **13**, 1071–1085 (2021).
12. J. Monte *et al.*, (2020). Biorefinery of Dunaliella salina: Sustainable recovery of carotenoids, polar lipids and glycerol. *Bioresource Technology*, **297**, 122509 https://doi.org/10.1016/j.biortech.2019.122509
13. A. Ben-Amotz, A. Katz, M. Avron, Accumulation of β-carotene in halotolerant algae: Purification and characterization of β-carotene-rich globules from *Dunaliella bardawil* (Chlorophyceae). *J. Phycol.* **18**, 529–537 (1982).
14. T. Varsano, S. G. Wolf, U. Pick, A chlorophyll *a/b*-binding protein homolog that is induced by iron deficiency is associated with enlarged photosystem I units in the eucaryotic alga *Dunaliella salina*. *J. Biol. Chem.* **281**, 10305–10315 (2006).
15. J. E. W. Polle *et al.*, Draft nuclear genome sequence of the halophilic and Beta-carotene-accumulating green alga *Dunaliella salina* strain CCAP19/18. *Genome Announc.* **5**, e01105-17 (2017).
16. L. Yao *et al.*, RNA-Seq transcriptomic analysis with Bag2D software identifies key pathways enhancing lipid yield in a high lipid-producing mutant of the non-model green alga *Dunaliella tertiolecta*. *Biotechnol. Biofuels* **8**, 191 (2015).
17. H. Shin *et al.*, Elucidation of the growth delimitation of *Dunaliella tertiolecta* under nitrogen stress by integrating transcriptome and peptidome analysis. *Bioresour. Technol.* **194**, 57–66 (2015).
18. H. M. Baker, B. F. Anderson, E. N. Baker, Dealing with iron: Common structural principles in proteins that transport iron and heme. *Proc. Natl. Acad. Sci. U.S.A.* **100**, 3579–3583 (2003).
19. M. Fisher, A. Zamir, U. Pick, Iron uptake by the halotolerant alga *Dunaliella* is mediated by a plasma membrane transferrin. *J. Biol. Chem.* **273**, 17553–17558 (1998).
20. M. Schwarz, N. Sal-Man, A. Zamir, U. Pick, A transferrin-like protein that does not bind iron is induced by iron deficiency in the alga *Dunaliella salina*. *Biochim. Biophys. Acta.* **1649**, 190–200 (2003).
21. L. A. Lambert, H. Perri, P. J. Halbrooks, A. B. Mason, Evolution of the transferrin family: Conservation of residues associated with iron and anion binding. *Comp. Biochem. Physiol. B Biochem. Mol. Biol.* **142**, 129–141 (2005).
22. Y. Paz, A. Katz, U. Pick, A multicopper ferroxidase involved in iron binding to transferrins in *Dunaliella salina* plasma membranes. *J. Biol. Chem.* **282**, 8658–8666 (2007).
23. E. Kazamia *et al.*, Endocytosis-mediated siderophore uptake as a strategy for Fe acquisition in diatoms. *Sci. Adv.* **4**, eaar4536 (2018).
24. E. Keshtacher-Liebson, Y. Hadar, Y. Chen, Oligotrophic bacteria enhance algal growth under iron-deficient conditions. *Appl. Environ. Microbiol.* **61**, 2439–2441 (1995).
25. S. S. Merchant, J. D. Helmann, Elemental economy: Microbial strategies for optimizing growth in the face of nutrient limitation. *Adv. Microb. Physiol.* **60**, 91–210 (2012).
26. E. Massé, C. K. Vanderpool, S. Gottesman, Effect of RyhB small RNA on global iron use in *Escherichia coli*. *J. Bacteriol.* **187**, 6962–6971 (2005).
27. E. Massé, S. Gottesman, A small RNA regulates the expression of genes involved in iron metabolism in *Escherichia coli*. *Proc. Natl. Acad. Sci. U.S.A.* **99**, 4620–4625 (2002).
28. C. E. Blaby-Haas, S. S. Merchant, Iron sparing and recycling in a compartmentalized cell. *Curr. Opin. Microbiol.* **16**, 677–685 (2013).
29. E. Knight, R. W. F. Hardy, Isolation and characteristics of Flavodoxin from nitrogen-fixing *Clostridium pasteurianum*. *J. Biol. Chem.* **241**, 2752–2756 (1966).
30. S. W. Ragsdale, L. G. Ljungdahl, Characterization of ferredoxin, flavodoxin, and rubredoxin from *Clostridium formicoaceticum* grown in media with high and low iron contents. *J. Bacteriol.* **157**, 1–6 (1984).
31. A. K. Singh, H. Li, L. A. Sherman, Microarray analysis and redox control of gene expression in the cyanobacterium *Synechocystis* sp. PCC 6803. *Physiol. Plant* **120**, 27–35 (2004).
32. D. E. Laudenbach *et al.*, Isolation, sequence analysis, and transcriptional studies of the flavodoxin gene from *Anacystis nidulans* R2. *J. Bacteriol.* **170**, 258–265 (1988).
33. J. La Roche, P. W. Boyd, R. M. L. McKay, R. J. Geider, Flavodoxin as an in situ marker for iron stress in phytoplankton. *Nature* **382**, 802–805 (1996).
34. J. J. Pierella Karlusich, A. F. Lodeyro, N. Carrillo, The long goodbye: The rise and fall of flavodoxin during plant evolution. *J. Exp. Bot.* **65**, 5161–5178 (2014).
35. C. E. Blaby-Haas, S. S. Merchant, Comparative and functional algal genomics. *Annu. Rev. Plant Biol.* **70**, 605–638 (2019).
36. S. Pagani, G. Vecchio, S. Iametti, R. Bianchi, F. Bonomi, On the role of the 2Fe-2S cluster in the formation of the structure of spinach ferredoxin. *Biochim. Biophys. Acta. Protein Struct. Mol. Enzymol.* **870**, 538–544 (1986).
37. V. Vidova, Z. Spacil, A review on mass spectrometry-based quantitative proteomics: Targeted and data independent acquisition. *Anal. Chim. Acta.* **964**, 7–23 (2017).
38. M. Medina, M. Martínez-Júlvez, J. K. Hurley, G. Tollin, C. Gómez-Moreno, Involvement of glutamic acid 301 in the catalytic mechanism of ferredoxin-NADP+ reductase from *Anabaena* PCC 7119. *Biochemistry* **37**, 2715–2728 (1998).
39. J. Wang *et al.*, Multi-metal restriction by Calprotectin impacts *de novo* Flavin biosynthesis in *Acinetobacter baumannii*. *Cell Chem. Biol.* **26**, 745–755.e7 (2019).
40. J. A. Raven, M. C. W. Evans, R. E. Korb, The role of trace metals in photosynthetic electron transport in O_2-evolving organisms. *Photosynthesis Res.* **60**, 111–150 (1999).
41. J. Barber, J. Nield, J. Duncan, T. S. Bibby, "Accessory chlorophyll proteins in cyanobacterial Photosystem I" in *Photosystem I* (Springer, Dordrecht, 2006), pp. 99–117.
42. T. Kobayashi, N. K. Nishizawa, Iron uptake, translocation, and regulation in higher plants. *Annu. Rev. Plant. Biol.* **63**, 131–152 (2012).
43. X. Gao, C. Bowler, E. Kazamia, Iron metabolism strategies in diatoms. *J. Exp. Bot.* **72**, 2165–2180 (2021).
44. C. E. Blaby-Haas, S. S. Merchant, The ins and outs of algal metal transport. *Biochim. Biophys. Acta.* **1823**, 1531–1552 (2012).
45. E. I. Urzica *et al.*, Systems and trans-system level analysis identifies conserved iron deficiency responses in the plant lineage. *Plant Cell* **24**, 3921–3948 (2012).
46. S. Kumar, G. Stecher, M. Suleski, S. Blair Hedges, TimeTree: A resource for timelines, timetrees, and divergence times. *Mol. Biol. Evol.* **34**, 1812–1819 (2017).
47. J. B. McQuaid *et al.*, Carbonate-sensitive phytotransferrin controls high-affinity iron uptake in diatoms. *Nature* **555**, 534–537 (2018).
48. C. S. Hassler, V. Schoemann, C. M. Nichols, E. C. V. Butler, P. W. Boyd, Saccharides enhance iron bioavailability to Southern Ocean phytoplankton. *Proc. Natl. Acad. Sci. U.S.A.* **108**, 1076–1081 (2011).
49. L. Davidi, E. Shimoni, I. Khozin-Goldberg, A. Zamir, U. Pick, Origin of β-carotene-rich plastoglobuli in *Dunaliella bardawil*. *Plant Physiol.* **164**, 2139–2156 (2014).
50. M. Mirdita *et al.*, ColabFold: Making protein folding accessible to all. *Nat. Methods* **19**, 679–682 (2022).
51. G. E. Crooks, G. Hon, J.-M. Chandonia, S. E. Brenner, WebLogo: A sequence logo generator. *Genome Res.* **14**, 1188–1190 (2004).
52. D. M. Emms, S. Kelly, OrthoFinder: Phylogenetic orthology inference for comparative genomics. *Genome Biol.* **20**, 1–14 (2019).
53. C. Camacho *et al.*, BLAST+: Architecture and applications. *BMC Bioinf.* **10**, 421 (2009).
54. S. D. Gallaher *et al.*, High-throughput sequencing of the chloroplast and mitochondrion of *Chlamydomonas reinhardtii* to generate improved *de novo* assemblies, analyze expression patterns and transcript speciation, and evaluate diversity among laboratory strains and wild isolates. *Plant J.* **93**, 545–565 (2018).
55. N. Sa, R. Rawat, C. Thornburg, K. D. Walker, S. Roje, Identification and characterization of the missing phosphatase on the riboflavin biosynthesis pathway in *Arabidopsis thaliana*. *Plant J.* **88**, 705–716 (2016).
56. S. D. Gallaher, L. Davidi, S. S. Merchant, calculate_exon_intron_sizes. Zenodo. https://doi.org/10.5281/zenodo.7719065. Deposited 10 March 2023.
57. S. D. Gallaher, L. Davidi, S. S. Merchant, Dunaliella salina Bardawil genome sequencing. Short Read Archive. https://www.ncbi.nlm.nih.gov/bioproject/PRJNA914849. Deposited 21 December 2022.
58. S. D. Gallaher, L. Davidi, S. S. Merchant, Dunaliella tertiolecta genome sequencing. Short Read Archive. https://www.ncbi.nlm.nih.gov/bioproject/PRJNA914763. Deposited 21 December 2022.
59. S. D. Gallaher, L. Davidi, S. S. Merchant, Gene Expression in Dunaliella salina Bardawil +/– Iron. Gene Expression Omnibus. https://www.ncbi.nlm.nih.gov/geo/query/acc.cgi?acc=GSE222140. Deposited 04 January 2023.
60. S. D. Gallaher, L. Davidi, S. S. Merchant, Gene Expression in Dunaliella tertiolecta +/– Iron. Gene Expression Omnibus. https://www.ncbi.nlm.nih.gov/geo/query/acc.cgi?acc=GSE222141. Deposited 04 January 2023.